RSC Advances

PAPER

View Article Online
View Journal | View Issue

Cite this: *RSC Adv.*, 2016, **6**, 2489

Solid-state, individual dispersion of single-walled carbon nanotubes in ionic liquid-derived polymers and its impact on thermoelectric properties†

Motohiro Nakano,[a] Yoshiyuki Nonoguchi,*[a] Takuya Nakashima,[a] Kenji Hata[b] and Tsuyoshi Kawai*[a]

Received 1st December 2015
Accepted 17th December 2015

DOI: 10.1039/c5ra25490f

www.rsc.org/advances

The structure of carbon nanotubes and their electronic interaction with a matrix are important for extracting the unprecedented electronic properties, which have yet to be explored. Here we investigate the dispersibility of single-walled carbon nanotubes (SWNTs) in ionic liquid-derived polymers (PILs), revealed by cross-sectional transmission electron microscopy, infrared optical spectroscopy, and Raman spectroscopy. Surprisingly, SWNTs studied here are highly dispersed, at least down to 7.5 nm-fibres, in a trimethylammonium-suspended PILs. Based on this discovery, we found that the well-dispersed and almost fully dispersed SWNTs in PILs are responsible for the enhanced thermoelectric properties, a future energy harvesting technique.

Introduction

The solid-state dispersion of single-walled carbon nanotubes (SWNTs) is a key step to create high-performance polymer composites.[1–3] SWNTs are usually dispersed in polymers in the form of bundles because of the strong van der Waals force. The poor dispersibility of SWNTs makes it difficult to investigate the electronic properties of individual SWNTs in the composites. Recently, highly-pure, millimeter-long, yet moderately dispersible SWNTs are now manufactured efficiently.[4] These characteristics have been applied in the development of electrical and thermal conductors.[5] However, the effect of dispersion on electronic properties is not well understood. In order to exploit the intrinsic, or unraveled properties, the creation of individually-dispersed SWNT networks in polymer matrices through controlled chemical interaction is required. Their large surface area (>1000 m^2 g^{-1}) offers various possible affinity to surrounding media.

Here we explore the solid-state dispersion of SWNTs in the matrix of ionic liquid-derived polymers. Ionic liquids are well-known dispersants of SWNTs.[6] Although most SWNT–polymer composites are composed of bundled SWNTs,[7–10] the partial dispersion of SWNT bundles into thinner ones has been demonstrated in ionic liquids and their polymers (PILs).[3,6] The specific interactions between SWNTs and ionic liquids are considered to overcome the attractive force between SWNTs in the bundles.[11]

In this study we demonstrate the complete isolation of bundles and show that the composite containing isolated SWNTs possesses the enhanced thermoelectric voltage. Thermoelectrics is an energy harvesting technique that generates power across temperature difference. Nanotube–polymer composites have been fabricated to exploit the potential, and/or unprecedented thermoelectric properties. For example, Chen *et al.* have demonstrated the thermoelectric nanocarbon composites with insulating polymer such as polystyrene, and conducting polymers such as PEDOT:PSS.[12–14] In contrast to the previous works, we found the dramatic enhancement of thermoelectric properties using insulating and ionic polymers with weak but specific affinity. We associate this thermo-voltage enhancement with nanotube–matrix interaction.

Results and discussion

We used SWNTs synthesized by the super-growth method, denoted as SG-CNTs, with relatively large diameters (~3 nm).[4,5] We prepared the SG-CNT/PIL composites, in which the SWNT bundles were well dispersed and isolated at the single CNT level. The initial flakes of SG-CNTs were composed of highly entangled fibres with a mean diameter of roughly 25 nm (Fig. S1†). In order to prepare uniform viscous dispersion, we used a grinding method rather than sonication. In the preparation of these samples, SG-CNTs and the monomers (**1–6**, Scheme 1) were ground with AIBN, forming "buckygels".[3,6] After thermal solidification at 333 K under vacuum, we obtained the samples as black solids (Fig. 1a). The polymerization was confirmed by FTIR (Fig. S2†). In an IR absorption spectrum

[a]*Graduate School of Materials Science, Nara Institute of Science and Technology, NAIST, Ikoma 630-0192, Japan. E-mail: nonoguchi@ms.naist.jp; tkawai@ms.naist.jp*
[b]*CNT-Application Research Center, National Institute of Advanced Science and Technology, AIST, Tsukuba 305-8565, Japan*

† Electronic supplementary information (ESI) available. See DOI: 10.1039/c5ra25490f

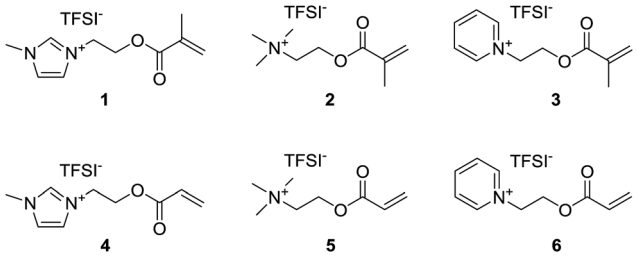

Scheme 1 Monomer structures. TFSI: bis(trifluoromethanesulfonyl) imide.

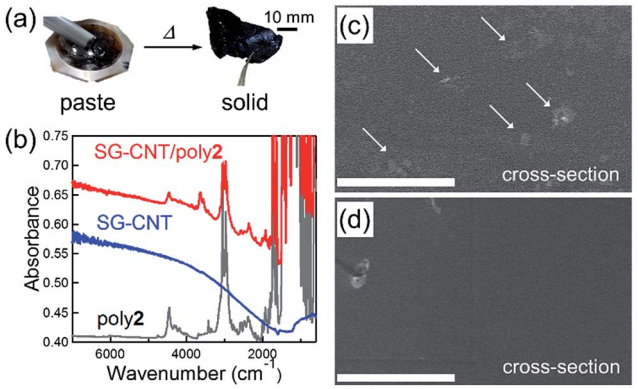

Fig. 1 (a) Photograph of 1 wt%-SG-CNT/poly**2**. (b) Infrared absorption spectra of poly**2**, SG-CNTs, and their composites. Cross-sectional scanning electron micrograph of (c) SG-CNT/poly**1** and (d) SG-CNT/poly**2**. Scale bars indicate 20 μm.

(Fig. 1b), the poly**2** composite showed a broad band-gap absorption of SG-CNTs and sharp vibrational absorption bands of poly**2**. The clearly distinguishable SG-CNTs infrared absorption bands suggested the suppressed inter-tube interactions of SG-CNTs in poly**2**. Since the IR spectrum was obtained in a transmission mode experiment, the observation of clear IR bands also indicated the suppressed interference with optical scattering from the bundles and the progress in their dispersion.

In order to evaluate the degree of dispersion of nanotube bundles, their cross section morphology was observed using scanning electron microscopy (SEM) at 1 kV acceleration voltage with a 3 nm spatial resolution. We found clear differences in the roughness of the cross sections dependent on the kind of polymers (Fig. 1c and d). The SG-CNT/poly**1** composite showed a relatively rough cross-section. Large amounts of SG-CNT bundles in the composite seems to be responsible for the inhomogeneity of the surface morphology. The contrastingly smooth cross section of a SG-CNT/poly**2** composite suggested that the bundles were highly dispersed in the poly**2** matrix at the nm-scale, down to roughly single tube levels.

For further investigation of the morphology, we performed transmission electron microscopy (TEM) on 100 nm-thick samples which were prepared by cutting the bulk samples with an ultra-microtome at 213 K. TEM observation revealed that the morphology of SG-CNTs is dependent on PILs. SG-CNTs in poly**1**, which were observed as white tubular shadows 3 nm in diameter, form many bundles larger than 50 nm in diameter (Fig. 2a). We also observed partially dispersed SG-CNTs in poly**3** (Fig. 2b). In contrast, SG-CNTs were surprisingly well dispersed down to single tube levels in poly**2** (Fig. 2c–e). Typically, long isolated SG-CNTs were dispersed and networked in poly**2** as depicted by arrows in Fig. 2d. We also found isolated open holes of ~3 nm in diameter (Fig. 2e), which were assigned to the round slices of isolated SG-CNTs cut by the microtome. The different dispersibility of SG-CNTs in poly**1**–**3** might be ascribed to different affinities between SG-CNTs and the cationic parts of polymers. That is, a trimethyl-ammonium cation seems to be efficient for dispersing SWNT bundles in comparison with the aromatic cations such as imidazolium and pyridinium. This tendency might be typical for SG-CNTs, considering the efficient solubilization of SWNTs with imidazolium-derived ILs reported by Aida and Fukushima.[3,6] We also studied the effects of main-

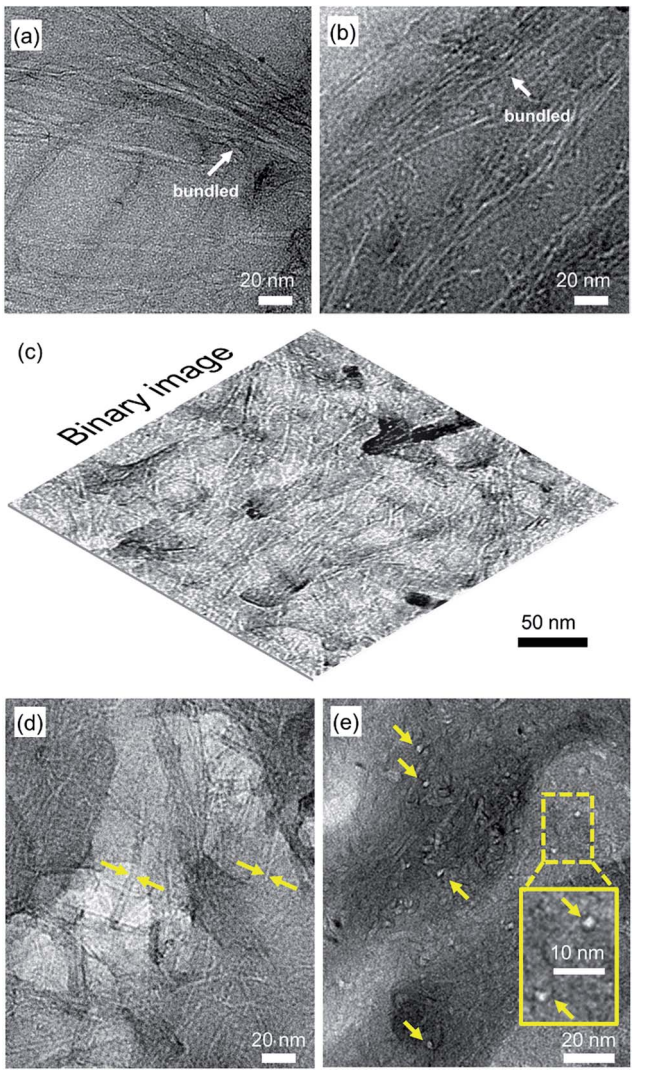

Fig. 2 Cross-sectional TEM images of (a) SG-CNT/poly**1** and (b) SG-CNT/poly**3**. Scale bars indicate 20 nm. Cross-sectional SEM images of SG-CNT/poly**2** composites at (c) low magnification and (d and e) high magnification.

chain structures and found a lower dispersibility of SG-CNTs in polyacrylate (poly**5**, Fig. S3†) than in corresponding polymethacrylate, poly**2**.

X-ray diffraction (XRD) analysis was employed to characterize the stacking of SWNTs, where peaks at high ($2\theta = 40$–$45°$) and low ($2\theta = 20$–$30°$) angle regions reflect the hexagonal packing structures of SWNTs in the bundles. Typically, clear (002) and (100) diffractions were observed at about $2\theta = 25°$ and $2\theta = 43°$ in raw SG-CNTs (Fig. S5†).[15] The SG-CNT/poly**2** composite showed almost no diffractions while poly**2** showed characteristic peaks derived from the self-organised structure of ILs. These observations clearly indicate that the hexagonally-packed SG-CNT bundles were mostly dispersed in a poly**2** matrix.

For further insight into the structure of SG-CNTs in the composites, we measured their Raman spectra (Fig. 3 and S6†). All the samples showed a typical G-band at about 1589 cm^{-1}. It should be noted that the Breit–Wigner–Fano (BWF) line around 1565 cm^{-1} in the Raman spectrum of the composites was smaller than those of the parent SG-CNTs. Since the BWF components originate from aggregated metallic SWNTs,[16,17] the BWF mode reflects aggregation of SWNTs. Similar spectrum narrowing has been observed for the surfactant-assisted dispersion of isolated SWNTs.[18] The present suppressed BWF modes in the composites are thus indicative of weakened interaction between nanotubes. Since the wavenumber of a G-band was maintained for all samples, charge transfer was not dominantly induced in the PIL matrices.

Creating efficient thermoelectric materials composed of low toxic elements with bendability and stability is still challenging, which is highly required for use in ambient conditions at temperature range lower than 400 K. SWNTs are a promising candidate for future light-weight, bendable thermoelectric powering materials, because of their nanoporous, flexible, and highly conducting nature. Herein we investigated the effect of dispersion on the electrical and thermoelectric properties of SWNT/PIL composites. As the loading level of SG-CNTs was increased, electrical conductivity increased (Fig. 4a). A poly**2** composite showed higher conductivity than a poly**5** composite. Considering the percolation model, composites with higher dispersibility should exhibit conducting percolation threshold at a lower loading level. Therefore, the improved conductivity of poly**2** composites is attributable to the dispersibility of SG-CNTs in poly**2** being higher than in poly**5**. These composites also showed significant concentration-dependent enhancement in the Seebeck coefficient (α), a measure of thermoelectric properties. In particular, poly**2** composites showed an increased Seebeck coefficient of 135 μV K^{-1} which is more than twice the raw SG-CNTs (Fig. 4b). The SG-CNT/poly**2** composite exhibited a further increase in Seebeck coefficients up to 150 μV K^{-1} at 340 K (Fig. 4c).

We calculated the power factor of SG-CNTs dispersed in poly**2** and poly**5** (Fig. 5). Due to increases in the Seebeck coefficient and electrical conductivity, we obtained the enhanced power factor ($\alpha^2\sigma$) using poly**2**, where SG-CNTs were highly

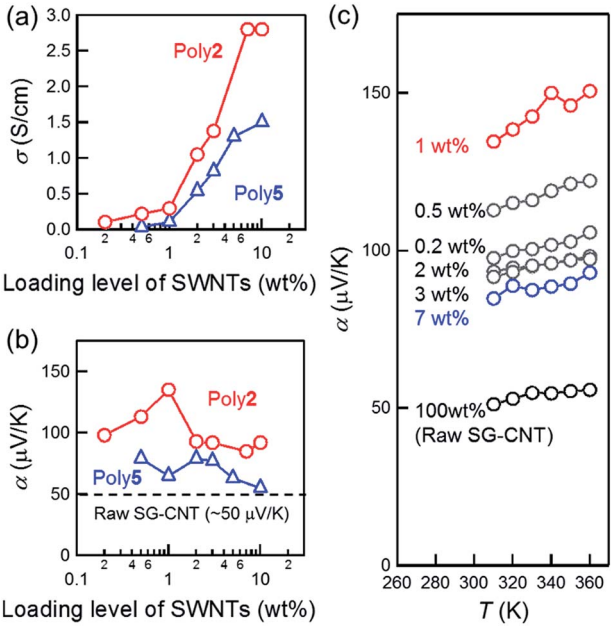

Fig. 4 Loading level dependence of (a) electrical conductivity and (b) Seebeck coefficients of SG-CNTs dispersed in poly**2** and poly**5** at 310 K. (c) Temperature dependence of Seebeck coefficient of SG-CNT-filled poly**2** composites at a different loading level (0.2–7 wt%, and 100 wt% (raw CNTs)). Details of other polymer composites are summarized in Fig. S6.† α is the Seebeck coefficient.

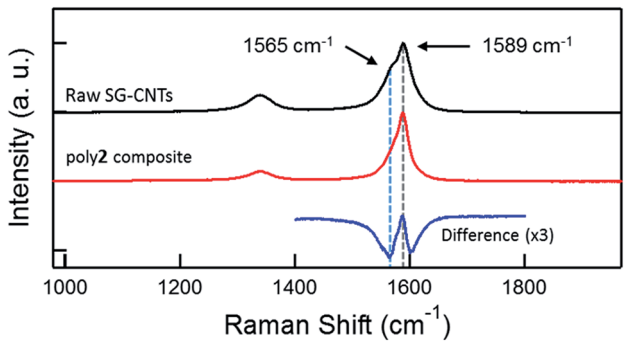

Fig. 3 Raman shift of raw SG-CNTs (black line) and SG-CNTs/poly**2** composites (red line) at 1 wt% of a loading level. Blue line indicates the difference between raw SG-CNTs and SG-CNTs/poly**2** composites.

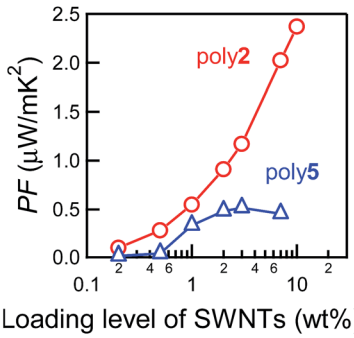

Fig. 5 Power factor of SG-CNTs dispersed in poly**2** and poly**5** at 310 K.

dispersed. Since nanotube concentration decreased down to less than 10 wt%, the absolute value of electrical conductivity and then power factor were relatively low.[19] The important point is that the efficient dispersion of SG-CNTs in the solid matrix might be beneficial for extracting excellent thermoelectric properties. For the practical application, completely dispersed SG-CNT/PIL composites with higher CNT concentration are highly desirable in the future work.

In order to verify the hypothesis above, this enhancement in the Seebeck coefficient of SG-CNTs was then analyzed from the viewpoint of dispersibility. The bundle thickness of SG-CNTs, which was evaluated by analysing cross-sectional TEM images in Fig. 2, can be interpreted as their dispersibility in polymers. It is expected that, based on hexagonal packing of nanotubes and their diameters of ~3 nm, encapsulated SG-CNTs exist in larger than ~10 nm-thick bundles.[20–22] For evaluating the degree of isolated nanotubes, we statistically counted the number of bundles thinner than 7.5 nm in diameter (Fig. 6a). To further confirm the efficient dispersion of CNTs in poly**2**, we also counted the number of intersections between bundles in every 1 μm-square on the TEM micrographs by means of the ImageJ software.[23] The mean intersection density was evaluated as a typical index number of dispersibility of nanotubes. We observed the highest degree of dispersibility of CNTs in poly**2** and a systematic increase in the Seebeck coefficient with an increase in the mean intersection density (Fig. 6b and S8†). We therefore concluded that thinner bundle formation with ionic liquids contributes to the enhancement in Seebeck coefficient of SWNT/PIL composites.

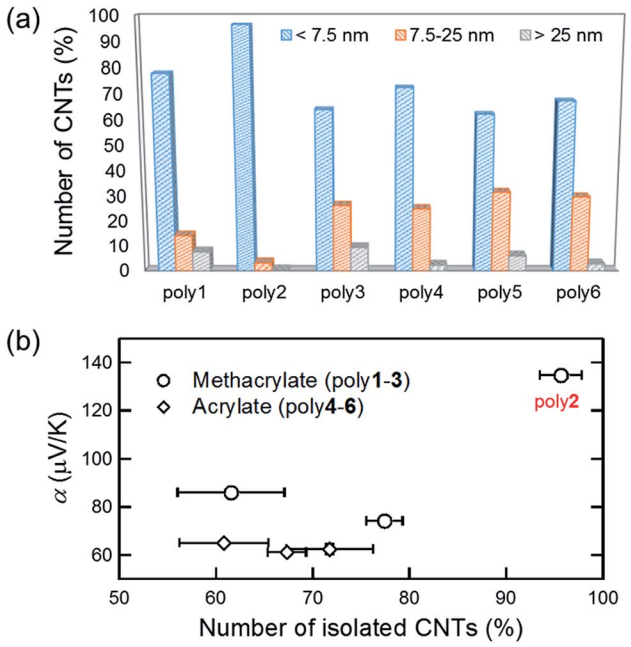

Fig. 6 Relationship between dispersibility and thermoelectricity of poly**1**–**6** composites with SG-CNTs at 1 wt% of a loading level. (a) Histogram of the number of isolated and bundled SWNTs. (b) Seebeck coefficient as function of the ratio of isolated tubes and thin bundles less than 7.5 nm in diameter.

Since α is closely associated with the gradient of the density-of-state (DOS) at the Fermi level,[24] SWNTs are expected to show relatively high α values because of their low dimensional electronic state and the narrow distribution of DOS. SWNTs actually show an α of 20–60 μV K^{-1}, which is significantly larger than that of multi-walled carbon nanotubes.[25] Since most available SWNTs are mixtures of those which have different diameters and chirality in their rolled-graphene structure, considerable interest has been focused on exploring the intrinsic thermoelectric nature of SWNTs. In this regard, α of a single-strand, and metallicity-soted SWNT has been estimated above 100 μV K^{-1}.[26–30]

Regarding the effects of π–π interaction between π-conjugated compounds on their electric properties, the enhanced Seebeck coefficient can be explained in terms of the low dimensionality of electronic states. The isolated SWNTs could have narrower DOS distribution supporting the enhancement in the Seebeck coefficient. Another possible explanation arises from the viewpoint of temperature difference across the inter-SWNT junctions. Since each bundle should have relatively large thermal transport capability in the SWNTs composites, the net temperature difference originates predominantly from local temperature difference at the junctions between bundles. The apparent Seebeck coefficient of the bulk films might thus be dominated across the junctions. The insertion of appropriate organic and inorganic compounds at the junctions can thus modulate the Seebeck effect.[31–35] Specific CH–π interaction between PILs and SWNTs might contribute not only to the SWNT dispersion but also to the efficient modulation of the selective transfer of positively charged carriers across the junctions.

Also, we would like to mention the possibility of flexible thermoelectric modules using the present SWNT-based materials. Our preliminary studies revealed that the SG-CNT/PIL composites exhibited moderate flexibility and almost no degradation of conductivity after repeated bending tests (Fig. S9†).

Conclusions

We found that large-diameter SWNTs can individually be dispersed in ionic liquid-bearing polymers. The deposition of PILs onto large-diameter SWNT buckypapers dramatically improved their thermoelectric properties. SG-CNTs exhibit the relatively large Seebeck coefficient in the ionic polymer composites tested, which is close to those of semiconductor-enriched SWNTs. Based on the present result, we are currently investigating the development of SWNT-ionic liquid hybrid materials showing the high Seebeck coefficient and electrical conductivity. Also, future SWNT-based thermoelectric materials need low thermal conductivity with high power factors ($\alpha^2\sigma$). Although SWNTs possess intrinsically high thermal conductivity, their assemblies might show relatively-low values (κ = 0.05–10 W mK^{-1}).[36] Our discovery will contribute to the development of thermoelectric power modules with industrially-available SWNTs.

Experimental

Materials

Reagents and solvents were used as received. 2-Bromoethanol, methacryloyl chloride, acryloyl chloride, 1-methylimidazole, dehydrated pyridine, silver nitrate ($AgNO_3$), super dehydrated acetonitrile, AIBN, deuterated chloroform ($CDCl_3$, 99.9%), dimethyl sulfoxide-d_6 (DMSO-d_6, 99.9%) were purchased from Wako Pure Chemical Industries. [2-(Methacryloyloxy)ethyl] trimethylammonium chloride (80 wt% in H_2O solution) and [2-(acryloyloxy)ethyl] trimethylammonium chloride (80 wt% in H_2O solution) were purchased from Sigma-Aldrich. Triethylamine, dichloromethane (CH_2Cl_2), methanol, and anhydrous magnesium sulfate ($MgSO_4$) were obtained from Nacalai Tesque. Lithium bis(trifluoromethanesulfonyl) imide (LiTFSI) and tetrahydrofurane (THF, dehydrated) were supplied from Kanto Chemical.

Synthesis of 2-bromoethyl methacrylate (7)

A mixture of 2-bromoethanol (4.21 mL, 59.8 mmol) and triethylamine (12.5 mL, 90.4 mmol) in THF (50 mL) was added dropwise to methacryloyl chloride (5.75 mL, 57.3 mmol) in THF (10 mL) of at 0 °C. The mixture was then stirred for four hours under argon atmosphere. The reaction mixture was evaporated at room temperature. The residue was diluted using CH_2Cl_2, and washed successively with water and brine. The organic layers were dried with $MgSO_4$, and then evaporated at room temperature. The resulting yellowish product was subjected to vacuum distillation (1.1 Torr, 54–57 °C) giving a colorless liquid (3.17 g, 16.4 mmol, yield: 28.6%). ^{1}H NMR (300 MHz, $CDCl_3$): δ (ppm) 6.22–6.13 (m, 1H; *H*CH=C), 5.75–5.57 (m, 1H; HC*H*=C), 4.46 (t, J = 6.1 Hz, 2H; CH_2–O), 3.56 (t, J = 6.1 Hz, 2H; N–CH_2), 2.02–1.90 (m, 3H; CH_3).

Synthesis of 2-bromoethyl acrylate (8)

Compound **8** was synthesized using a procedure similar to **7**, giving a colourless liquid (7.13 g, 37.0 mmol, yield: 96.0%). ^{1}H NMR (300 MHz, $CDCl_3$): δ (ppm) 6.59–6.41 (m, 1H; C=C*H*), 6.26–6.09 (m, 1H; *H*CH=C), 5.90 (dd, J = 10.4, 1.3 Hz, 1H; HC*H*=C), 4.48 (t, J = 6.1 Hz, 2H; CH_2–O), 3.56 (t, J = 6.2 Hz, 2H; N–CH_2).

Synthesis of 1-[2-(methacryloyloxy)ethyl]-pyridinium bromide (9)

A 3.51 mL (25.2 mmol) solution of **7** in acetonitrile (20 mL) was added dropwise to pyridine (2.00 mL, 24.9 mmol) under argon atmosphere. The mixture was then stirred at 85 °C for 16 hours. The solution was allowed to cool to room temperature and the solvent was removed by rotary evaporation. The residue was used in the following step without further purification.

Synthesis of 3 as a typical procedure for the synthesis of ionic liquid monomers

7.72 g (26.9 mmol) of LiTFSI in a small amount of aqueous solution was added into **9** in aqueous solution at 0 °C and stirred for one hour. The residue was extracted with CH_2Cl_2 at least three times. Excess salt and HBr were removed by mixing the resulting liquid with water until no bromide anion was detected by observing the color change of $AgNO_3$ aqueous solution (5 mM). The organic layer was dried over $MgSO_4$ and then evaporated under reduced pressure. The yellowish residue was redissolved in methanol and activated carbon was added to the mixture, which was then let stand overnight in the refrigerator. The mixture was filtered on a membrane filter with 0.2 μm pores. The filtrate was evaporated to remove the solvent and set under high vacuum at 60 °C for 24 hours to give a viscous colorless liquid (8.10 g, 17.1 mmol, yield: 68.6%). For **3**, ^{1}H NMR (300 MHz, DMSO-d_6): δ (ppm) 9.19–9.09 (m, 2H; C$H_{Pyr\text{-}o}$), 8.66 (td, J = 7.8, 1.5 Hz, 1H; C$H_{Pyr\text{-}p}$), 8.21 (t, J = 6.4 Hz, 2H; C$H_{Pyr\text{-}m}$), 6.00 (d, J = 0.9 Hz, 1H; HC*H*=C), 5.74–5.67 (m, 1H; *H*CH=C), 5.02–4.92 (m, 2H; CH_2–O), 4.66–4.57 (m, 2H; N–CH_2), 1.81 (d, J = 0.9 Hz, 3H; CH_3).

Synthesis of 1, 4 and 6

Compound **1** was synthesized a procedure similar to **3**, except for the use of imidazole units. **4** and **6** were synthesized similar to **3** except for the use of 1-methylimidazole, and dehydrated pyridine, respectively, with **8**. For **1**, ^{1}H NMR (300 MHz, DMSO-d_6): δ (ppm) 9.15 (s, 1H; N–C*H*=N), 7.79–7.71 (dt, J = 1.7 Hz, 2H; N–C*H*–C*H*=N), 6.07–6.03 (m, 1H; *H*CH=C), 5.72 (t, J = 1.6 Hz, 1H; HC*H*=C), 4.56–4.49 (m, 2H; CH_2–O), 4.47–4.42 (m, 2H; N–CH_2), 3.87 (s, 3H; N–CH_3), 1.87–1.84 (m, 3H; C=C–CH_3); for **4**, ^{1}H NMR (300 MHz, DMSO-d_6): δ (ppm) 9.15 (s, 1H; N–C*H*=N), 7.83–7.72 (m, 2H; N–C*H*–C*H*=N), 6.33 (d, J = 1.6 Hz, 1H; C=C*H*), 6.25–6.10 (m, 1H; *H*CH=C), 6.04–5.97 (m, 1H; HC*H*=C), 4.58–4.50 (m, 2H; CH_2–O), 4.49–4.43 (m, 2H; N–CH_2), 3.87 (s, 3H; N–CH_3); for **6**, ^{1}H NMR (300 MHz, DMSO-d_6): δ (ppm) 9.16–9.06 (m, 2H; C$H_{Pyr\text{-}o}$), 8.70–8.60 (m, 1H; C$H_{Pyr\text{-}p}$), 8.24–8.15 (m, 2H; C$H_{Pyr\text{-}m}$), 6.35–6.27 (m, 1H; C=C*H*), 6.18–6.06 (m, 1H; *H*CH=C), 6.01–5.94 (m, 1H; HC*H*=C), 4.99–4.91 (m, 2H; CH_2–O), 4.67–4.60 (m, 2H; N–CH_2).

Synthesis of 2 and 5

Compound **2**, and **5** were obtained by reacting [2-(methacryloyloxy)ethyl] trimethylammonium chloride and [2-(acryloyloxy)ethyl] trimethylammonium chloride, respectively, with LiTFSI. The mixture was purified following a manner similar to **3**. For **2**, ^{1}H NMR (300 MHz, DMSO-d_6): δ (ppm) 6.09 (d, J = 0.9 Hz, 1H; *H*CH=C), 5.80–5.74 (m, 1H; HC*H*=C), 4.53 (br s, 2H; CH_2–O), 3.74–3.67 (m, 2H; N–CH_2), 3.13 (s, 9H; N–(CH_3)$_3$), 1.91 (d, J = 1.1 Hz, 3H; C=C–CH_3); for **5**, ^{1}H NMR (300 MHz, DMSO-d_6): δ (ppm) 6.44–6.35 (m, 1H; C=C*H*), 6.26–6.15 (m, 1H; *H*CH=C), 6.08–6.00 (m, 1H; HC*H*=C), 4.61–4.50 (m, 2H; CH_2–O), 3.76–3.67 (m, 2H; N–CH_2), 3.13 (s, 9H; N–(CH_3)$_3$).

Film preparation

CNTs were dried overnight under vacuum at 120 °C before use. Ionic liquid monomers were added to a methanol solution containing 2 wt% of AIBN and this mixture was deaerated for three hours under vacuum, followed by grinding the mixture with SWNTs for five minutes. Then, the mixture was dried

under vacuum for 10 minutes, after which the mixture was solidified by radical polymerization at 60 °C for 2 hours. Buckypapers without any dispersant were prepared by filtrating SWNT dispersion on a membrane filter as reference samples. These films were dried overnight under vacuum at 60 °C before use.

Characterization

SEM images were taken by Hitachi SU-6600 at 2 kV of accelerating voltage. Bright-field TEM images of polymer composites were obtained at 300 kV with a JEOL JEM-3100FEF electron microscope. Samples were ultra-microtomed with a diamond knife on a Leica Ultracut UCT microtome at −60 °C to give sections with a nominal thickness of 100 nm. The specimens on carbon-coated Cu microgrids were transferred to the TEM vacuum chamber. DC electrical conductivity was measured using the four-point probe method (Mitsubishi Chemical Analytech Loresta GP Model MCP-T610). Thermopower was recorded using a Seebeck coefficient measurement system (MMR technologies K20SB100-3R) with a Joule–Thomson effect temperature controller.[37] Samples were cut roughly into a rectangular shape (5 mm in length and 2 mm in width). These were then transferred to, and stuck on a sample stage of the measurement system using conducting silver pastes. Raman spectroscopy was performed at an excitation wavelength of 532 nm with JASCO NRS-5100. Infrared absorption spectra were measured using Bruker Optics HYPERION2000 with TENSOR II FTIR. ^{1}H NMR spectra were recorded at room temperature using a JEOL AL-300 spectrometer (300 MHz).

Acknowledgements

We thank Prof. Takeharu Haino (Hiroshima University) for his valuable comments on molecular interaction. This work was financially supported by JSPS KAKENHI, Grant-in-Aid for Young Scientists (B) (grant number 26790014), and NAIST Green Photonics Research Project (MEXT). This work made use of NAIST common facilities supported by MEXT Nanotechnology Platform Japan program.

Notes and references

1 V. A. Davis, A. N. G. Parra-Vasquez, M. J. Green, P. K. Rai, N. Behabtu, V. Prieto, R. D. Booker, J. Schmidt, E. Kesselman, W. Zhou, H. Fan, W. W. Adams, R. H. Hauge, J. E. Fischer, Y. Cohen, Y. Talmon, R. E. Smalley and M. Pasquali, *Nat. Nanotechnol.*, 2009, **4**, 830–834.

2 M. Okamoto, T. Fujigaya and N. Nakashima, *Adv. Funct. Mater.*, 2008, **18**, 1776–1782; T. Fujigaya and N. Nakashima, *Adv. Mater.*, 2013, **25**, 1666–1681; M. R. Berber, T. Fujigaya, K. Sasaki and N. Nakashima, *Sci. Rep.*, 2013, **3**, 1764.

3 T. Fukushima, A. Kosaka, Y. Yamamoto, T. Aimiya, S. Notazawa, T. Takigawa, T. Inabe and T. Aida, *Small*, 2005, **2**, 554–560.

4 K. Hata, D. N. Futaba, K. Mizuno, T. Namai, M. Yumura and S. Iijima, *Science*, 2004, **306**, 1362–1364.

5 S. Ata, M. Yumura, K. Kobashi and K. Hata, *Nano Lett.*, 2012, **12**, 2710–2716.

6 T. Fukushima, A. Kosaka, Y. Ishimura, T. Yamamoto, T. Takigawa, N. Ishii and T. Aida, *Science*, 2003, **300**, 2072–2074.

7 Q. Yao, L. Chen, W. Zhang, S. Liufu and X. Chen, *ACS Nano*, 2010, **4**, 2445–2451.

8 Y. Choi, Y. Kim, S.-G. Park, Y.-G. Kim, B. J. Sung, S.-Y. Jang and W. Kim, *Org. Electron*, 2011, **12**, 2120–2125.

9 C. A. Hewitt, A. B. Kaiser, S. Roth, M. Craps, R. Czerw and D. L. Carroll, *Nano Lett.*, 2012, **12**, 1307–1310.

10 K. Suemori, Y. Watanabe and S. Hoshino, *Appl. Phys. Lett.*, 2015, **106**, 113902.

11 J. Wang, H. Chu and Y. Li, *ACS Nano*, 2008, **2**, 2540–2546.

12 G. Sun, G. Chen, J. Liu, J. Yang, J. Xie, Z. Liu, R. Li and X. Li, *Polymer*, 2009, **50**, 5787–5793.

13 G. Sun, G. Chen, Z. Liu and M. Chen, *Carbon*, 2010, **48**, 1434–1440.

14 Z. Zhang, G. Chen, H. Wang and X. Li, *Chem.–Asian J.*, 2015, **10**, 149–153.

15 D. N. Futaba, T. Yamada, K. Kobashi, M. Yumura and K. Hata, *J. Am. Chem. Soc.*, 2011, **133**, 5716–5719.

16 M. Paillet, P. Poncharal, A. Zahab, J.-L. Sauvajol, J. C. Meyer and S. Roth, *Phys. Rev. Lett.*, 2005, **94**, 237401.

17 K. Kempa, *Phys. Rev. B: Condens. Matter Mater. Phys.*, 2002, **66**, 195406.

18 A. M. Rao, J. Chen, E. Richter, U. Schlecht, P. C. Eklund, R. C. Haddon, U. D. Venkateswaran, Y.-K. Kwon and D. Tománek, *Phys. Rev. Lett.*, 2001, **86**, 3895–3898.

19 K. Xu, G. Chen and D. Qiu, *J. Mater. Chem. A*, 2013, **1**, 12395–12399.

20 D. Golberg, Y. Bando, L. Bourgeois, K. Kurashima and T. Sato, *Carbon*, 2000, **38**, 2017–2027.

21 A. Peigney, C. Laurent, E. Flahaut, R. R. Bacsa and A. Rousset, *Carbon*, 2001, **39**, 507–514.

22 U. J. Kim, H. R. Gutiérrez, J. P. Kim and P. C. Eklund, *J. Phys. Chem. B*, 2005, **109**, 23358–23365.

23 H. W. Morrison and J. A. Filosa, *J. Neuroinflammation*, 2013, **10**, 4.

24 M. Cutler and N. F. Mott, *Phys. Rev.*, 1969, **181**, 1336–1340.

25 C. A. Hewitt and D. L. Carroll, *Chem. Phys. Lett.*, 2013, **580**, 67–72.

26 J. P. Small, K. M. Perez and P. Kim, *Phys. Rev. Lett.*, 2003, **91**, 256801.

27 C. Yu, L. Shi, Z. Yao, D. Li and A. Majumdar, *Nano Lett.*, 2005, **5**, 1842–1846.

28 M. Piao, M.-K. Joo, J. Na, Y.-J. Kim, M. Mouis, G. Ghibaudo, S. Roth, W.-Y. Kim, H.-K. Jang, G. P. Kennedy, U. Dettlaff-Weglikowska and G.-T. Kim, *J. Phys. Chem. C*, 2014, **118**, 26454–26461.

29 Y. Nakai, K. Honda, K. Yanagi, H. Kataura, T. Kato, T. Yamamoto and Y. Maniwa, *Appl. Phys. Express*, 2014, **7**, 025103.

30 N. T. Hung, A. R. T. Nugraha, E. H. Hasdeo, M. S. Dresselhaus and R. Saito, *Phys. Rev. B: Condens. Matter Mater. Phys.*, 2015, **92**, 165426.

31 M. Ito, N. Okamoto, R. Abe, H. Kojima, R. Matsubara, I. Yamashita and M. Nakamura, *Appl. Phys. Express*, 2014, **7**, 065102.
32 Y. Nonoguchi, T. Murayama, M. Ishizaki, K. Kanaizuka, M. Kurihara, K. Hata and T. Kawai, *Chem. Lett.*, 2014, **43**, 1254–1256.
33 M. Nakano, Y. Nonoguchi, T. Nakashima and T. Kawai, *Jpn. J. Appl. Phys.*, 2015, **54**, 04DN03.
34 R. Matsuoka, R. Toyoda, R. Sakamoto, M. Tsuchiya, K. Hoshiko, T. Nagayama, Y. Nonoguchi, K. Sugimoto, E. Nishibori, T. Kawai and H. Nishihara, *Chem. Sci.*, 2015, **6**, 2853–2858.
35 Y. Nonoguchi, K. Hata and T. Kawai, *ChemPlusChem*, 2015, **80**, 1158–1163.
36 C. Cho, B. Stevens, J.-H. Hsu, R. Bureau, D. A. Hagen, O. Regev, C. Yu and J. C. Grunlan, *Adv. Mater.*, 2015, **27**, 2996–3001.
37 Y. Nonoguchi, K. Ohashi, R. Kanazawa, K. Ashiba, K. Hata, T. Nakagawa, C. Adachi, T. Tanase and T. Kawai, *Sci. Rep.*, 2013, **3**, 3344.